Analyst

Accepted Manuscript

ROYAL SOCIETY OF CHEMISTRY

www.rsc.org/analyst

Journal Name

RSCPublishing

ARTICLE

Significantly enhanced antibacterial activity of TiO_2 nanofibers with hierarchical nanostructures and controlled crystallinity

Won Seok Lee, Yang-Seok Park, and Yoon-Kyoung Cho*

Cite this: DOI: 10.1039/x0xx00000x

Received 00th January 2012,
Accepted 00th January 2012

DOI: 10.1039/x0xx00000x

www.rsc.org/

Recently, there has been increased interest in electrospun-titanium dioxide nanofibers (TiO_2 NFs) as antibacterial agents owing to their advantages, such as simple and cost-effective fabrication processes, and high surface areas. However, the photocatalytic effects of TiO_2 NFs are relatively low because of their low-ordered crystalline structure, and the antibacterial effect is only effective under UV illumination owing to their large band-gap energy. In this paper, we demonstrated significantly enhanced antibacterial activity of hierarchical anatase TiO_2 NFs against *Staphylococcus aureus* in the presence of UV light. Furthermore, the uniform deposition of a large quantity of Ag nanoparticles on the surface of the TiO_2 NFs ensured a significant enhancement of the antibacterial performance, even under dark conditions. These results were obtained by exploiting the enhanced photocatalytic effect achieved through control of the crystallinity, as well as the enhanced surface area, of the nanomaterials.

Introduction

Titanium dioxide (TiO_2) is one of the most popular antibacterial materials[1] used in broad applications, including water purification, implantable devices, air-conditioning filters, *etc*., because of its strong photo-oxidation activity,[2] long-term chemical and physical stability,[3, 4] and self-cleaning effects.[5] The antibacterial performance of TiO_2 is further enhanced in nanoscale materials owing to a high surface-to-volume ratio, as the photochemical reaction mainly occurs on the surfaces. TiO_2 nanoparticles (NPs) have shown enhanced antibacterial effects because of their high surface area compared with TiO_2 thin films.[7] For example, Lan *et al.* showed that both biocompatibility and antibacterial activity were enhanced on TiO_2 nanotubes with electron-beam evaporated Ag.[6] Gupta *et al.* investigated the antibacterial effects of TiO_2 and Ag doped TiO_2 NPs prepared by sol-gel method and demonstrated that both *Escherichia coli* and *Staphylococcus aureus* showed zero viability at 60 mg of Ag-doped (7%) TiO_2 in 30 mL of culture.[8] However, the difficulty in separating TiO_2 NPs after a photochemical reaction limits their practical applications.[9] Furthermore, the easy aggregation of TiO_2 NPs in the solution decreases their photocatalytic efficiency because of the reduced surface area.

To overcome these limitations, TiO_2 nanofibers (NFs) were fabricated using the relatively easy, fast, and low-cost electrospinning (ES) technique.[10] TiO_2 NFs are particularly attractive because of their mesoporous membrane structure.[11] TiO_2 NFs are not only stable in solution without aggregation, but are also easily separated and collected from the solution after photochemical reactions. However, the photocatalytic efficiency of the TiO_2 NFs is relatively low and only effective under UV illumination because of their low-ordered crystalline structure and large band-gap energy.[12]

One of the most promising approaches to overcome these limitations is the use of noble metal or semiconductor-coupled TiO_2 nanocomposites.[13-16] It has been demonstrated that the deposition of Ag can enhance the antibacterial capability of TiO_2 under visible light by promoting electron-hole separation. This effect originates from an ability to trap electrons in the Schottky barrier at the Ag/TiO_2 interface, therefore reducing the recombination rate of electrons and holes.

Furthermore, Ag itself acts as an antimicrobial agent even under dark conditions.[14, 21] For example, Zhang *et al.*[14] evaluated the antibacterial effect of Ag-TiO_2 thin films against *Escherichia coli* and *Staphylococcus aureus*; the films showed excellent antimicrobial performance under both UV light irradiation and in dark environments. However, long reaction times (3–24 h) were required to achieve effective antibacterial activity because of the limited contact area of the film.

In an effort to increase the surface area of the Ag-coupled TiO_2, Jin *et al.* used a co-electrospinning method, but Ag ions were easily oxidized to Ag_2O after the pyrolysis step. Pant *et al.*[22] developed Ag/TiO_2 NF membranes that had surfaces decorated with Ag NPs using a photoreduction method.[23-25] Although this composite structure showed enhanced antibacterial activity compared with the previously reported film-type substrate, the antibacterial activity was not significantly enhanced, possibly because the amount of Ag loading was relatively small and the deposition was not uniform.[13,22]

Despite these previous efforts, there is still a need to develop more effective and facile methods to fabricate Ag-TiO_2 nanocomposites for photocatalytic and antibacterial applications. One of the critical challenges is the development of a novel method to prepare well-dispersed active Ag with maximum loading density without sacrificing the surface area. The hierarchical structure of TiO_2 NFs[26-28] with higher surface area and improved photocatalytic effect can be alternative way to solve the drawbacks as mentioned above. In this work, we have developed a facile two-step fabrication method to further enhance the surface area of electrospun TiO_2 NFs

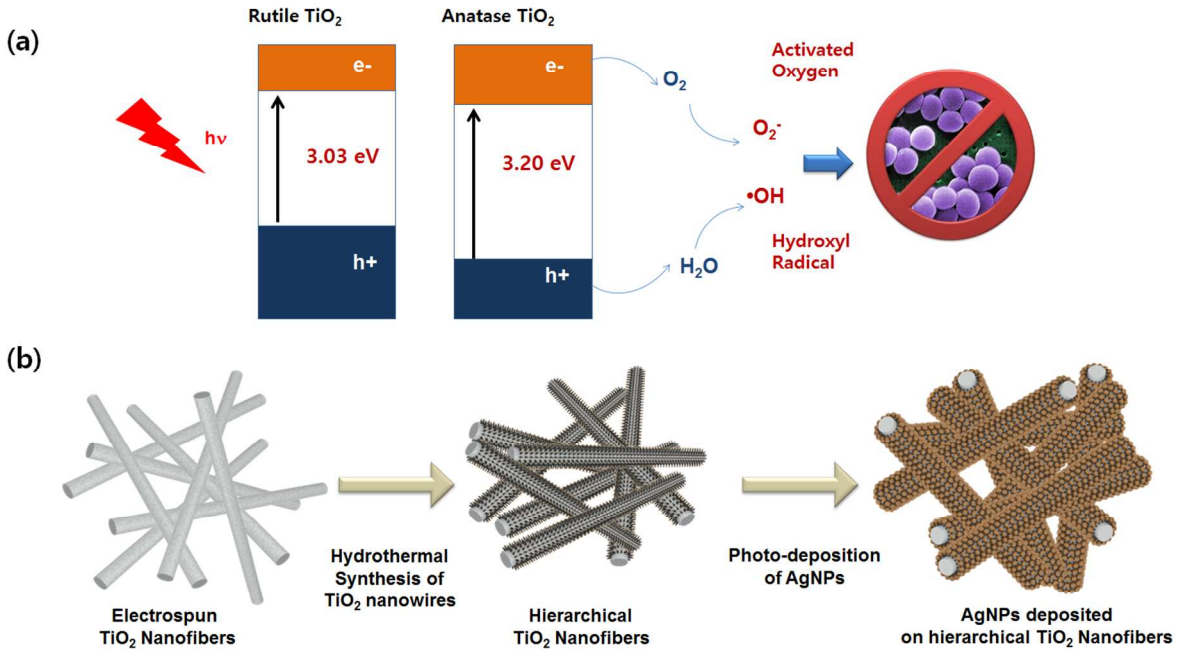

Fig. 1 Schematic illustration of the approaches used to achieve enhanced antibacterial activity of TiO_2 NFs (a) by controlling the crystalline phase and (b) by hierarchical structures prepared by electrospinning, pyrolysis, hydrothermal synthesis of nanowires, and deposition of Ag NPs.

by subsequent hydrothermal synthesis of TiO_2 nanowires (NWs). As illustrated in **Fig. 1**, we investigated the significant enhancement of antibacterial activity, not only by making the hierarchical nanostructure of TiO_2 NWs on TiO_2 NFs, but also by controlling the crystallinity of TiO_2 (rutile or anatase phases) of both the NWs and NFs. We further investigated the photo-deposition of Ag NPs by utilizing the photocatalytic effects of the hierarchical TiO_2 nanomaterials with various crystalline phases. As a result, a large amount of Ag NPs could be uniformly deposited on the surface of hierarchical anatase TiO_2 NFs with anatase TiO_2 NWs, which ensured a significant enhancement of the antibacterial performance, even under dark conditions.

Experimental

Materials: Titanium tetraisopropoxide (TTIP, 98%), polyvinylpyrrolidone (PVP, MW = 1,300,000), acetic acid, anhydrous ethanol (99.5+%), $Ti(OBu)_4$ (97%), potassium titanium oxide oxalate dehydrate (PTO, MW = 354.13), diethylene glycol (DEG, MW = 106.12), and $AgNO_3$ (MW = 169.87) were all purchased from Sigma-Aldrich. Hydrogen chloride (HCl, 35–37%) was purchased from Samchun.

Fabrication of pure and hierarchical TiO_2 nanofibers: Pure TiO_2 NFs were obtained by ES of TTIP/PVP NFs on Si substrate and subsequent calcination. First, a solution of TTIP (1.5 g) dissolved in ethanol (3 mL) and acetic acid (3 mL) was mixed with a solution containing 11 wt% PVP in ethanol. To fabricate TTIP/PVP NFs, the mixed solution was steadily introduced through a stainless steel needle onto a Si substrate as grounded substrate at a high DC-voltage of 15 kV, flow rate of 0.3 mL/h, and fixed distance of 10 cm. Finally, the TiO_2 NFs with anatase or rutile phases were obtained by calcination at 500 °C or 900 °C, respectively, for 3 h in air. The hierarchical structure of the TiO_2 NFs was obtained by hydrothermal synthesis of TiO_2 NWs with anatase or rutile phases on the surface of the TiO_2 NFs. The hydrothermal synthesis of TiO_2 NWs with an anatase structure was performed as follows: 15 mL deionized (DI) water and 25 mL DEG were mixed in a 150 mL Teflon-lined autoclave. Then, 0.025 M PTO was injected into the solution and stirred for 30 min. The TiO_2 NFs with anatase phase were immersed in the mixture at a specific angle to ensure that the TiO_2 NFs were facing downwards. This system was then sealed in an autoclave and heated at 150 °C for 6 h. Finally, the device was washed with DI water and ethanol. Similarly, for the synthesis of TiO_2 NWs with rutile phase, 50 mL DI water and 50 mL HCl were mixed in a 150 mL Teflon-lined autoclave. Then, 1.7 mL $Ti(OBu)_4$ was injected into this solution and stirred for 30 min. Following this, the TiO_2 NFs with rutile phase were immersed in the mixture at a specific angle to ensure that the TiO_2 NFs were facing downwards. This system was then sealed in an autoclave and heated at 150 °C for 6 h. Finally, the device was washed with DI water and ethanol.

Photodeposition of Ag NPs on the surface of TiO_2 NFs: TiO_2 NFs were immersed in 1 mM $AgNO_3$ and exposed to UV light with a power density of 1 kW for 3 min. Under UV irradiation, Ag NPs were deposited onto the surface of the TiO_2 NFs through a photoreduction process, in which positively charged Ag ions were reduced to Ag by the electrons generated in the TiO_2 NFs.

Characterization: Field-emission scanning electron microscopy (FE-SEM, FEI Nano230), high-resolution transmission electron microscopy (HR-TEM, JEM-2100F), normal transmission electron microscopy (Normal-TEM, JEM-2100), and energy dispersive spectrometry (EDS, JEM-2100F) were used for the microstructure

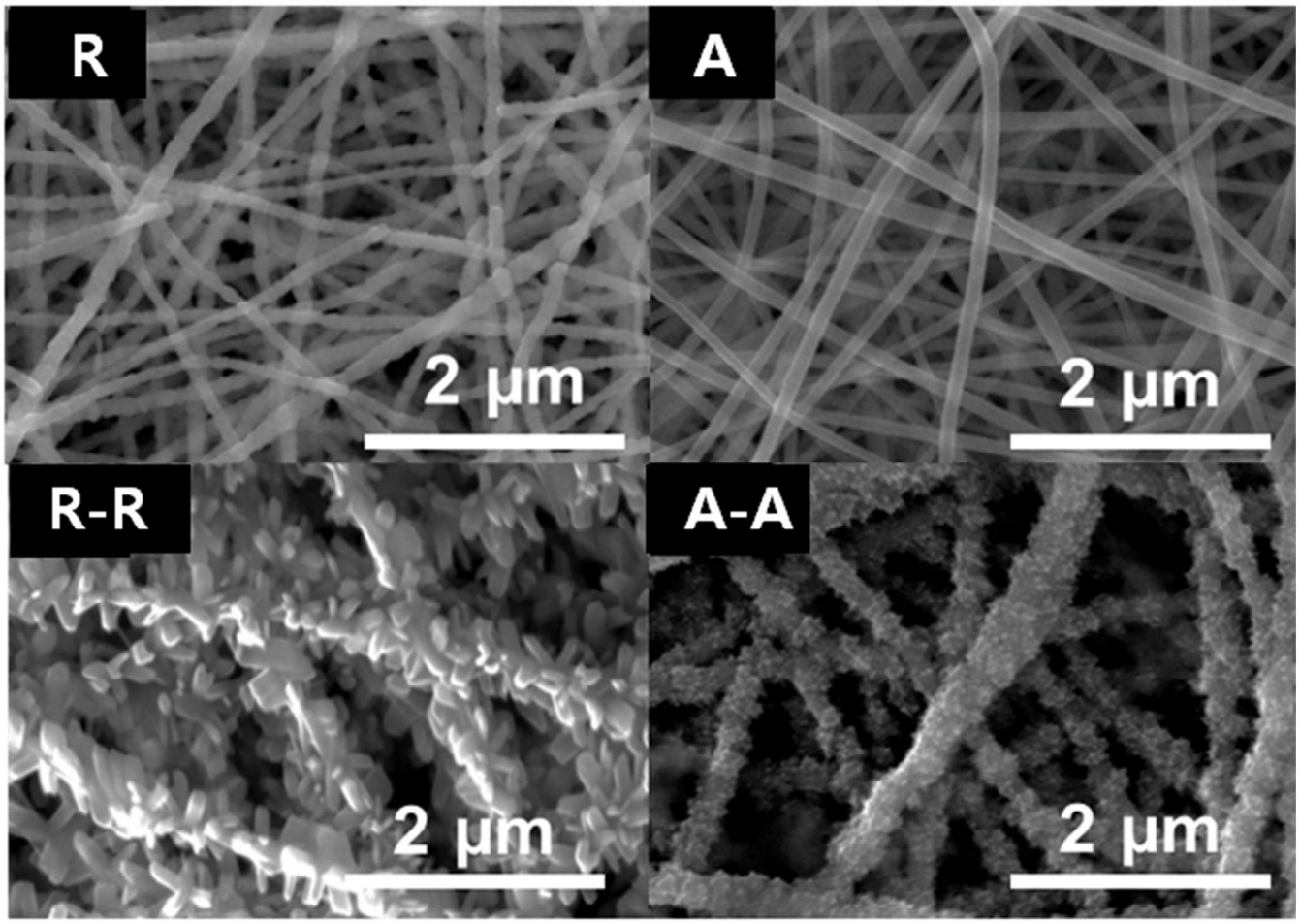

Fig. 2 SEM images of TiO_2 NFs with various crystalline phases and nanostructures: (R) pure TiO_2 NFs with rutile phase; (A) pure TiO_2 NFs with anatase phase; (R-R) hierarchical TiO_2 rutile NFs with rutile-TiO_2 NWs; and (A-A) hierarchical TiO_2 anatase NFs with anatase-TiO_2 NWs.

analysis of the TiO_2 NFs. X-ray diffraction (XRD, D8 Advance, Bruker) was used to confirm the crystal phases of the TiO_2 NFs and TiO_2 NWs.

Evaluation of antibacterial activity: The bacteria were cultivated in a Luria-Bertani (LB) broth medium at 37 °C for 24 h; the bacterial solution was then diluted to approximately 3×10^6 CFU/mL with the LB broth medium. The antibacterial activity against *S. aureus* was determined by quantitative evaluation in the presence of UV light and under dark conditions. For the former, 10 μL of the diluted bacterial solution was dropped onto the TiO_2 NFs placed in a sterilized Petri dish. The Petri dish was sealed and exposed for 90 s to UV light with a low intensity (0.7 mW/cm^2) at 365 nm. For the evaluation of the antibacterial activity under dark conditions, a similar system was prepared (10 μL of the diluted bacterial solution dropped on Ag-decorated TiO_2 NFs) and kept under dark conditions for 1 h. After these treatments, the solution containing bacteria was washed from the samples with 10 mL of LB broth in the Petri dish. Then, 100 μL of each bacteria suspension solution was transferred and spread on three nutrient agar plates. Following incubation at 37 °C for 24 h, the average number of surviving bacterial colonies on the three incubated agar plates was calculated. All samples were treated with oxygen plasma for 5 min to obtain hydrophilic surfaces before the antibacterial activation experiments.

Results and Discussions

In this work, the hierarchical TiO_2 NFs were prepared through a hydrothermal synthesis of TiO_2 NWs on pure TiO_2 NFs prepared via ES, followed by calcination. Images of the fabricated pure and hierarchical TiO_2 NFs are shown in **Fig. 2**. In particular, the crystalline phase of the pure TiO_2 NFs was controlled by a heat treatment, in which TiO_2 NFs with the rutile phase (R-TiO_2 NFs) and anatase phase (A-TiO_2 NFs) were obtained by calcination for 3 h at 900 °C or 500 °C, respectively. Increasing the calcination temperature to 900 °C promoted the conversion of the crystalline phase from anatase to rutile and an increase in grain size to ~70 nm, as the rutile phase is thermodynamically stable at grain sizes greater than 35 nm.[29] The grain size was analyzed from TEM image shown in Fig. S1.

The hierarchical TiO_2 NFs were obtained through an additional hydrothermal synthesis of TiO_2 NWs on the originally fabricated

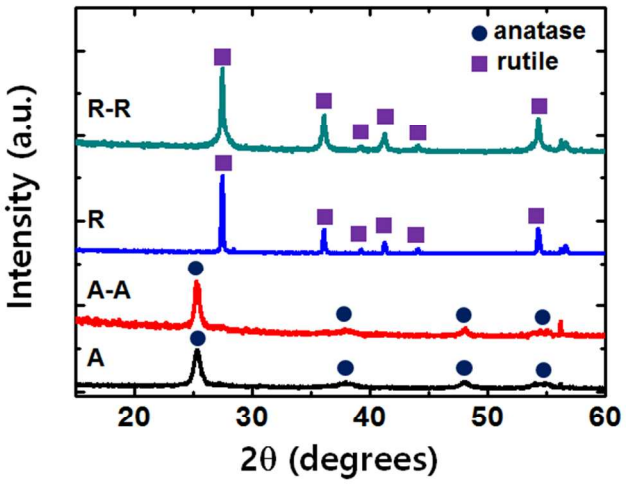

Fig. 3 XRD analysis of pure and hierarchical TiO_2 NFs: (A) pure TiO_2 anatase NFs prepared by electrospinning followed by calcination at 500 °C, and (A-A) hierarchical TiO_2 anatase NFs prepared by hydrothermal synthesis of TiO_2 NWs with anatase phase on top of the electrospun TiO_2 anatase NFs. These materials were well indexed as the anatase crystalline phase. (R) Pure TiO_2 rutile NFs prepared by electrospinning followed by calcination at 900 °C, and (R-R) hierarchical TiO_2 NFs prepared through hydrothermal synthesis of TiO_2 rutile NWs onto the rutile TiO_2 NFs. Both the pure and hierarchical TiO_2 materials were well indexed as the rutile crystalline phase.

pure TiO_2 NFs. Here, we monitored the crystalline phases of the synthesized TiO_2 NWs by controlling the precursor solution in the hydrothermal synthesis. In particular, the R-TiO_2 NWs were vertically grown on the R-TiO_2 NFs from a precursor solution containing $Ti(OBu)_4$, HCl, and water.[30] The synthesized R-TiO_2 NWs were found to have diameters of ~150 nm and lengths of ~200 nm. Similarly, A-TiO_2 NWs were vertically grown on the A-TiO_2 NFs from a precursor solution including PTO, DEG, and water.[31] The average diameter and length of the synthesized A-TiO_2 NWs were measured to be ~20 nm and ~80 nm, respectively.

Both HCl and DEG were employed to avoid hydrolysis of the precursor solutions and to support the directional growth of TiO_2 NWs on the TiO_2 NFs. The volume ratio of HCl/water and DEG/water is a critical factor for the synthesis of R-TiO_2 NWs and A-TiO_2 NWs. In particular, the following ratios were used in this study: water/HCl ratio of 50:50 *v/v* for R-TiO_2 NWs[30] and water/DEG ratio of 15:25 *v/v* for A-TiO_2 NWs.[31]

The crystalline phases of the pure and hierarchical TiO_2 NFs were characterized by XRD analysis in the two-theta range of 15–60° (**Fig. 3**). For the pure TiO_2 NFs, A-TiO_2 NFs were well indexed as the anatase crystal structure of TiO_2 (JCPDS card No. 84-1286), where the peaks at 25.48°, 37.88°, 48.18°, 54.68°, and 55.38° corresponded to the anatase crystal planes of (101), (004), (200), (105), and (211), respectively.[32] Additionally, R-TiO_2 NFs were well indexed as the rutile crystal structure of TiO_2 (JCPDS card No. 75-1753), where the peaks at 27.48°, 36.18°, 39.16°, 41.28°, 44.01°, and 54.18° corresponded to the rutile crystal planes of (110), (101), (200), (111), (210), and (211), respectively.[32] For the hierarchical TiO_2 NFs, A-A TiO_2 NFs and R-R TiO_2 NFs were well indexed as the anatase and rutile phases, respectively, without any secondary peaks. These data confirmed that both the A-TiO_2 and R-TiO_2 NWs were successfully synthesized using the methods discussed above.

The application of the pure and hierarchical TiO_2 NFs as antibacterial agents was demonstrated under UV illumination for a very short time of 1.5 min to confirm their enhanced photocatalytic effect owing to their increased surface area and controlled crystalline phase. The antibacterial activity of the pure and hierarchical TiO_2 NFs with different crystalline phases against *S. aureus* is illustrated in **Fig. 4.** A-A-TiO_2 NFs exhibited the highest antibacterial activity and R- TiO_2 NFs the lowest. The antibacterial performance of 89.90 ± 2.02% only after 1.5 minute of UV irradiation is significant enhancement compared to previous reports where 76.7 ± 3 % of antibacterial activity after 1 hr under UV light was reported[21] or 3 hrs of UV irradiation was required for effective antibacterial activity.[14]

The underlying mechanism of the antimicrobial activity of TiO_2 in the presence of UV light is relatively well established;[33] it is known, for instance, that reactive hydroxyl radicals generated by the photocatalysis of TiO_2 under UV illumination lead to cell death by reacting with cell membranes and DNA. Kubacka *et al.* recently reported the antimicrobial mechanism of TiO_2 film by analyzing the genome-wide expression profile analysis.[34] The high antibacterial activity of A-A-TiO_2 NFs was attributed to an increased number of hydroxyl radicals, resulting from an enhanced photocatalytic effect. A-A-TiO_2 NFs showed about 1.5 times higher antimicrobial activity compared with pure A-TiO_2 NFs or R-R-TiO_2 NFs. We believe that the enhanced photocatalytic effect of A-A-TiO_2 NFs originates from their higher surface area compared with that of pure A-TiO_2 NFs, as well as their lower recombination rate of electron-hole pairs compared with that of R-R-TiO_2 NFs.[35]

Next, the hierarchical Ag/TiO_2 NF composites were obtained by carrying out the photodeposition of Ag NPs on the TiO_2 NFs. The Ag NPs were deposited on the TiO_2 NFs through reduction of the positively charged Ag ions by the electrons generated by TiO_2 NFs in a solution of 10 mM $AgNO_3$ under UV irradiation.

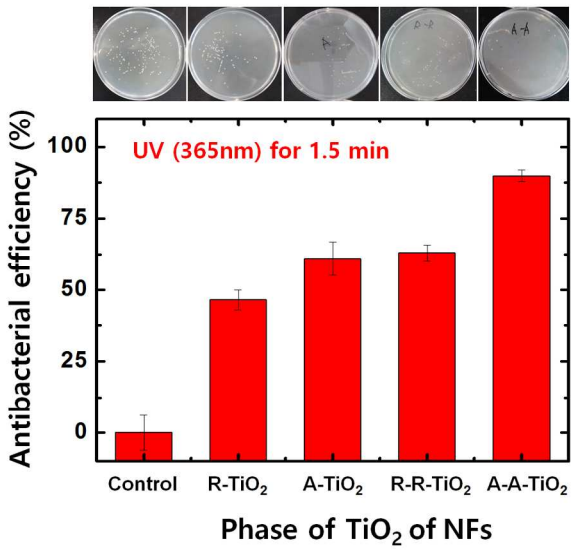

Fig. 4 Antibacterial activity of TiO_2 NFs under UV illumination: antibacterial efficiency of control, pure rutile TiO_2 NFs (R-TiO_2), pure anatase TiO_2 NFs (A-TiO_2), hierarchical rutile-rutile TiO_2 NFs (R-R-TiO_2), and hierarchical anatase-anatase TiO_2 NFs (A-A-TiO_2) against *S. aureus* under UV illumination for 1.5 min. The control is the Si substrate placed in a Petri dish under the same treatment conditions. The error bars represent ± standard error of the mean (s.e.m.).

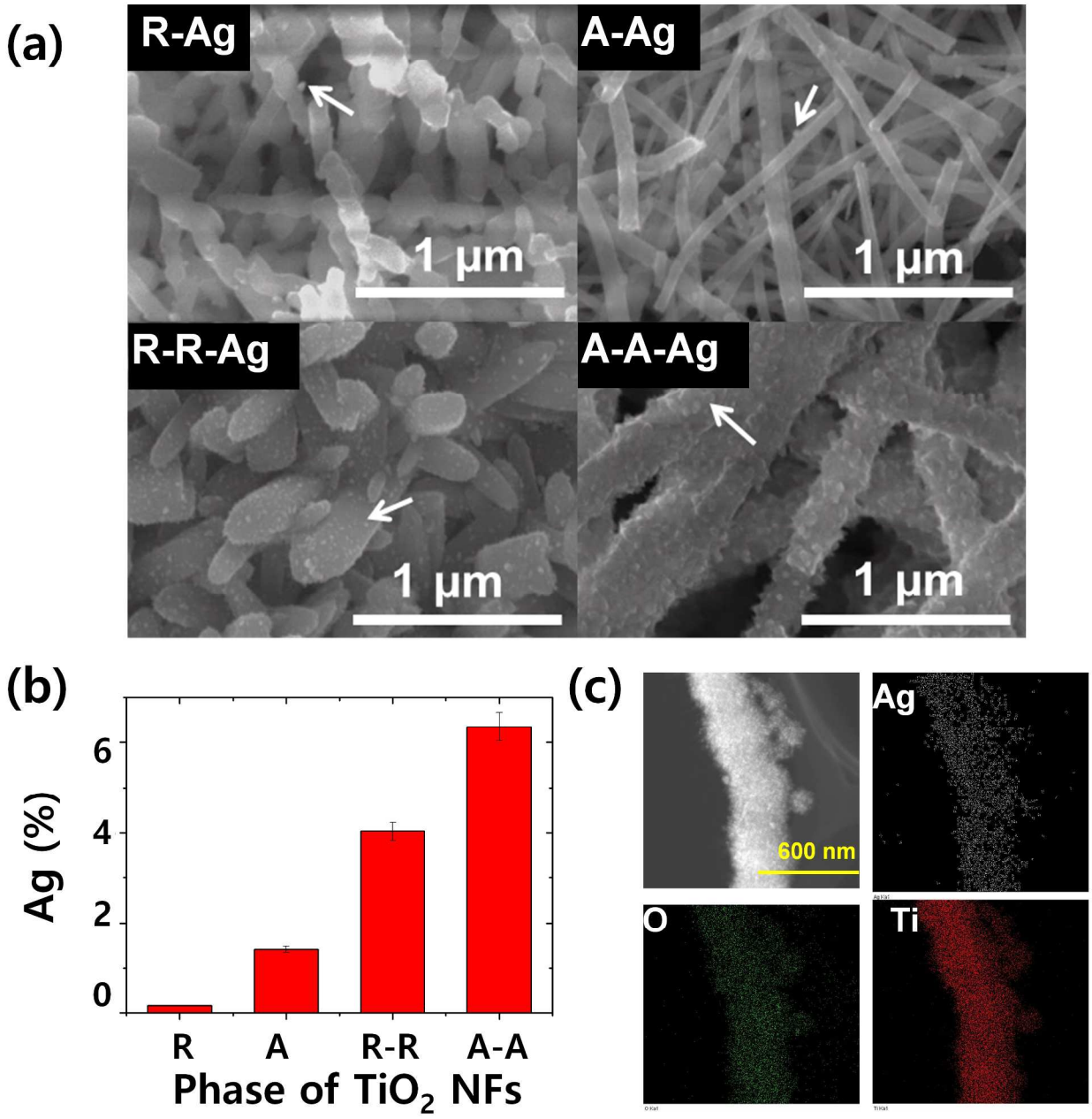

Fig. 5 Microstructure characterization of Ag-decorated TiO_2 NFs: (a) SEM analysis of (R-Ag) Ag-decorated pure TiO_2 rutile NFs, (A-Ag) Ag-decorated pure TiO_2 anatase NFs, (R-R-Ag) Ag-decorated hierarchical TiO_2 rutile NFs, and (A-A-Ag) Ag-decorated hierarchical TiO_2 anatase NFs, (b) the weight composition in Ag-decorated TiO_2 NFs is shown. (c) TEM-EDS analysis of Ag-decorated A-A-TiO_2 NFs showing the uniform distribution of Ag, O, and Ti.

The SEM images of Ag deposited on pure and hierarchical TiO_2 NFs are shown in **Fig. 5a**. The weight percent of the Ag NPs deposited on the pure and hierarchical TiO_2 NFs were determined by EDS analysis. As shown in **Fig. 5b**, among the pure TiO_2 NFs, A-TiO_2 NFs have a higher weight percent of Ag NPs than R-TiO_2 NFs. This difference was possibly caused by a higher photocatalytic effect in the A-TiO_2 NFs than in the R-TiO_2 NFs, resulting in an increase in the number of reduced positively charged Ag ions. This effect was attributed to the lower recombination rate of the anatase phase owing to its higher band-gap energy (3.20 eV) compared with that of the rutile phase (3.03 eV).[36] Most importantly, the Ag NPs were more densely deposited with an increased weight percent on the hierarchical TiO_2 NFs, indicating that the photocatalytic activity was enhanced by the increase of the surface area and the larger number of electrons available on the surface of the hierarchical TiO_2 NFs. In particular, A-A-TiO_2 NFs were found to have a higher weight percent of deposited Ag NPs than R-R-TiO_2 NFs (**Fig. 5b**), suggesting that A-A-TiO_2 NFs are the most photocatalytically active

among the pure and hierarchical TiO_2 NFs. The higher photocatalytic effect of A-A-TiO_2 NFs (compared with R-R-TiO_2 NFs) was attributed to a lower recombination rate and a higher surface area, which were a result of the smaller grain-size of the anatase phase compared with that of the rutile phase. High-magnification TEM-EDS images of Ag deposited A-A-TiO_2 NFs are shown in **Fig. 5c**. In comparison with the previous result that showed sparsely deposited Ag NPs on pure TiO_2 NFs,[13] these images indicate that the Ag NPs are densely and uniformly deposited on A-A-TiO_2 NFs. Detail weight percentage of each phase analyzed by SEM-EDS is shown in **Fig. S2**.

Finally, the Ag-deposited TiO_2 NFs were employed as antimicrobial agents under dark conditions for 1 h in order to test the inherent antibacterial effect of the Ag NPs, which originates from the reaction of silver ions with the membranes and DNA of cells.[21] The antibacterial activities of the TiO_2 NFs against *S. aureus* are illustrated in **Fig. 6.** While the TiO_2 NFs without Ag NPs rarely killed *S. aureus* in the absence of light, regardless of the crystallinity or nanostructure of the nanomaterials,[16] TiO_2 NFs decorated with Ag NPs exhibited effective antibacterial activity even under dark conditions. In particular, the results of this test showed that the antibacterial activity is related to the quantity of Ag NPs on the surface of the TiO_2 NFs. For example, the highest antibacterial activity (83.47 ± 0.87% of bacteria killed) was observed for 6.35 wt% Ag NPs deposited on A-A-TiO_2 NFs, which was significantly larger than that observed for 4.03 wt% Ag NPs deposited on R-R-TiO_2 (43.43 ± 8.33% of bacteria killed), 1.41 wt% Ag NPs deposited on A-TiO_2 (25.95 ± 2.87%), and 0.15 wt% Ag NPs deposited on R-TiO_2 (18.03 ± 3.00%).

This result indicates that the material with the highest content of Ag NPs showed the highest antibacterial activity against *S. aureus* under dark conditions. The mechanism of antibacterial activity of Ag NPs under dark conditions is known to involve cell death caused by Ag ions released from Ag NPs in the presence of water and oxygen.[37] Thus, based on these results, we concluded that the photocatalytic activity is significantly enhanced in A-A-TiO_2 NFs compared with pure TiO_2 NFs and hierarchical TiO_2 NFs with the rutile phase; an enhanced antimicrobial activity under dark conditions was obtained as a result of the uniform deposition and increased quantity of Ag NPs on the surface of A-A-TiO_2 NFs. It is also significantly higher antibacterial performance compared to previous report using Ag-TiO_2 composite nanofilms in which only 45 % of antibacterial activity was achieved.[21]

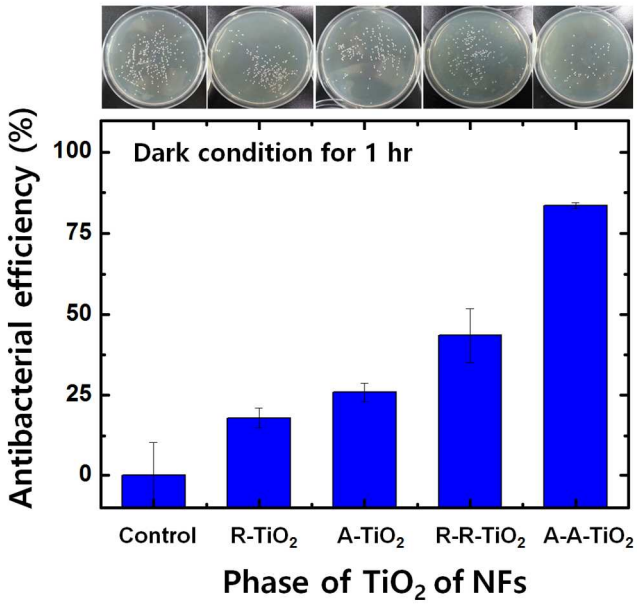

Fig. 6 Antibacterial activity of Ag-decorated TiO_2 NFs under dark conditions: the antibacterial efficiency of Ag-decorated pure rutile TiO_2 NFs (Ag-R-TiO_2), pure anatase TiO_2 NFs (Ag-A-TiO_2), hierarchical rutile-rutile TiO_2 NFs (Ag-R-R-TiO_2), and hierarchical anatase-anatase TiO_2 NFs (Ag-A-A-TiO_2) against *S. aureus* in the absence of light. The control is the Si substrate placed in a Petri dish under the same treatment. The error bars represent ± standard error of the mean (s.e.m.).

Conclusions

In this work, a novel hierarchical structure of anatase-TiO_2 NFs for enhanced antibacterial activity was prepared by combining ES followed by calcination with the hydrothermal synthesis of anatase-TiO_2 NWs on the surface of the anatase-TiO_2 NFs. This structure exhibited a highly enhanced photocatalytic effect owing to an increased surface area and an improved crystallinity of the surface. This enhanced photocatalytic effect led to a highly enhanced antibacterial activity of 89.90 ± 2.02% in the presence of UV light, even for a very short irradiation time (1.5 min). Furthermore, Ag/TiO_2 NF composites were prepared via photoreduction synthesis of Ag NPs that were deposited on the hierarchical anatase-TiO_2 NFs under UV illumination. Compared with the previously reported composite structure of Ag NPs sparsely deposited on pure TiO_2 NFs, our novel structure showed that Ag NPs could be uniformly and densely deposited on the hierarchical anatase-TiO_2 NFs due to the increased photocatalytic effect of this structure, which resulted in a highly enhanced antibacterial activity with 83.47 ± 0.87% of bacteria killed after 1 h under dark conditions. We are confident that our hierarchical TiO_2 anatase NFs, which show a highly enhanced photocatalytic effect resulting from the increased surface area and improved crystallinity, can be employed for their antimicrobial properties in a wide range of applications, such as biomedical or water treatments.

Acknowledgements

This work was supported by a National Research Foundation (NRF) grant (2013R1A2A2A05004314) and by the Korean Health Technology R&D Project, Ministry of Health & Welfare (A121994) funded by the Korean government.

Notes and references

Department of Biomedical Engineering, School of Life Sciences, Ulsan National Institute of Science and Technology (UNIST), Banyeon-ri 100, Ulsan 689-798, Republic of Korea.

*E-mail: ykcho@unist.ac.kr

References

1. A. Fujishima, T. N. Rao and D. A. Tryk, *J. Photochem. Photobiol., C*, 2000, **1**, 1-21.
2. A. Mills and S. Le Hunte, *J. Photochem. Photobiol., A*, 1997, **108**, 1-35.

3. R. Wang, K. Hashimoto, A. Fujishima, M. Chikuni, E. Kojima, A. Kitamura, M. Shimohigoshi and T. Watanabe, *Nature*, 1997, **388**, 431-432.
4. R. Wang, K. Hashimoto, A. Fujishima, M. Chikuni, E. Kojima, A. Kitamura, M. Shimohigoshi and T. Watanabe, *Adv. Mater.*, 1998, **10**, 135-138.
5. W.-K. Oh, S. Kim, M. Choi, C. Kim, Y. S. Jeong, B.-R. Cho, J.-S. Hahn and J. Jang, *ACS Nano*, 2010, **4**, 5301-5313.
6. M. -Y. Lan, C. -P. Liu, H. -H. Huang and S. -W. Lee, *PLoS ONE*, 2013, **8**, e75364
7. A. L. Linsebigler, G. Lu and J. T. Yates, *Chem. Rev.*, 1995, **95**, 735-758.
8. K. Gupta, R. P. Singh, A. Pandey and A. Pandey, *Beilstein J. Nanotechnol*, 2013, **4**, 345-351
9. H. Schmidt, M. Naumann, T. S. Müller and M. Akarsu, *Thin Solid Films*, 2006, **502**, 132-137.
10. W. E. Teo and S. Ramakrishna, *Nanotechnology*, 2006, **17**, R89.
11. X. Zhang, S. Xu and G. Han, *Mater. Lett.*, 2009, **63**, 1761-1763.
12. S. Xu, A. Li, G. Poirier and N. Yao, *Scanning*, 2012, **34**, 341-346.
13. L. Liu, Z. Liu, H. Bai and D. D. Sun, *Water Res.*, 2012, **46**, 1101-1112.
14. Q. Zhang, C. Sun, Y. Zhao, S. Zhou, X. Hu and P. Chen, *Environ. Sci. Technol.*, 2010, **44**, 8270-8275.
15. R. Dastjerdi, M. R. M. Mojtahedi, A. M. Shoshtari and A. Khosroshahi, *J. Text. Inst.,* 2009, **101**, 204-213.
16. S. H. Hwang, J. Song, Y. Jung, O. Y. Kweon, H. Song and J. Jang, *Chem. Commun.,* 2011, **47**, 9164-9166.
17. Z. Liu, D. D. Sun, P. Guo and J. O. Leckie, *Nano Lett.,* 2006, **7**, 1081-1085.
18. J. Moon, J.-A. Park, S.-J. Lee, T. Zyung and I.-D. Kim, *Sens. Actuators, B,* 2010, **149**, 301-305
19. H. Wang, T. You, W. Shi, J. Li and L. Guo, *J. Phys. Chem. C,* 2012, **116**, 6490-6494.
20. S. Wang, J. Bai, H. Liang, T. Xu, C. Li, W. Sun and H. Liu, *J. Dispersion Sci. Technol.,* 2013, **35**, 777-782.
21. B. Yu, K. M. Leung, Q. Guo, W. M. Lau and J. Yang, *Nanotechnology*, 2011, **22**, 115603.
22. H. R. Pant, D. R. Pandeya, K. T. Nam, W.-i. Baek, S. T. Hong and H. Y. Kim, *J. Hazard. Mater.*, 2011, **189**, 465-471.
23. A. Sclafani and J.-M. Herrmann, *Journal of Photochemistry and Photobiology A: Chemistry*, 1998, **113**, 181-188.
24. S. C. Chan and M. A. Barteau, *Langmuir*, 2005, **21**, 5588-5595.
25. D. Guin, S. V. Manorama, J. N. L. Latha and S. Singh, *J. Phys. Chem. C*, 2007, **111**, 13393-13397.
26. D. Sabba, S. Agarwala, S. Pramana and S. Mhaisalkar, *Nanoscale Res. Lett.,* 2014, **9**, 14.
27. C. Wang, X. Zhang, C. Shao, Y. Zhang, J. Yang, P. Sun, X. Liu, H. Liu, Y. Liu, T. Xie and D. Wang, *J. Colloid Interface Sci.*, 2011, **363**, 157-164.
28. W. S. Lee, Y.-S. Park and Y.-K. Cho, *ACS Appl. Mater. Interfaces*, 2014, **6**, 12189-12195.
29. A. Furube, T. Asahi, H. Masuhara, H. Yamashita and M. Anpo, *J. Phys. Chem. B*, 1999, **103**, 3120-3127.
30. C. Sun, N. Wang, S. Zhou, X. Hu, S. Zhou and P. Chen, *Chem. Commun.*, 2008, 3293-3295.
31. D. K. Roh, W. S. Chi, S. H. Ahn, H. Jeon and J. H. Kim, *ChemSusChem*, 2013, **6**, 1384-1391.
32. L. Jiang, Y. Zhong and G. Li, *Mater. Res. Bull.*, 2009, **44**, 999-1002.
33. K. Sunada, Y. Kikuchi, K. Hashimoto and A. Fujishima, *Environ. Sci. Technol.*, 1998, **32**, 726-728.
34. A. Kubacka, M. S. Diez, D. Rojo, R. Bargiela, S. Ciordia, I. Zapico, J. P. Albar, C. Barbas, V. A. P. M. Santos, M. F. -Garcıa and M. Ferrer, *Sci. Rep.*, 2014, **4**, 4134
35. A. Sclafani and J. M. Herrmann, *J. Phys. Chem.,* 1996, **100**, 13655-13661.
36. N. G. Park, J. van de Lagemaat and A. J. Frank, *J. Phys. Chem. B,* 2000, **104**, 8989-8994.
37. C. Hu, Y. Lan, J. Qu, X. Hu and A. Wang, *J. Phys. Chem. B*, 2006, **110**, 4066-4072.